

Evaluating the impact of floating spheres on evaporation reduction and water salinity control in reservoirs

Guo-chen Hao^{a,b}, Ke-Bin Shi^{a,b,*}, Ke-wu Han^{a,b}

^a College of Hydraulic and Civil Engineering, Xinjiang Agricultural University, Urumqi 830052, China

^b Xinjiang Key Laboratory of Hydraulic Engineering Security and Water Disasters Prevention, Urumqi 830052, China

ARTICLE INFO

Handling Editor - Dr R Thompson

Keywords:

Plain reservoir
Floating spheres
Evaporation
Water salinization

ABSTRACT

The construction of simple reservoirs in arid regions helps meet the water demands for agricultural irrigation, industry, and domestic use, while also alleviating local water shortages and related issues. However, environmental concerns associated with reservoir development are becoming more evident. For instance, the stored water is gradually becoming saline. Studies suggest that reducing water evaporation over extended periods can effectively lower the salt concentration in the water. Currently, there is limited research on salt migration in reservoir water when covered with anti-evaporation materials. Given the potential impact of these materials on the water environment and hydrodynamic conditions, this study seeks to examine the spatiotemporal distribution patterns of reservoir mineralization under such covering. To this end, laboratory and field experiments were conducted to analyze the impact of covering the water surface with floating high-density polyethylene spheres to reduce evaporation and its effect on water salinity. These experiments included monitoring water temperature, dissolved oxygen, pH, sediment resuspension, and water conductivity, as well as calculating the contribution of sediment release and evapotranspiration to the increase in salinity concentration within the water column. This study investigates the role of floating high-density polyethylene (HDPE) spheres in reducing reservoir evaporation and mitigating water salinity. Laboratory and field experiments assessed the effects of different coverage levels (0 %-74.98 %) on evaporation rates, sediment resuspension, and water chemistry. The findings indicate that covering 74.98 % of the reservoir surface led to a 28.97 % reduction in salinity ($p < 0.05$) over one irrigation cycle. Evaporation inhibition varied from 13.56 % to 60.19 %, depending on coverage. However, floating spheres exhibited reduced effectiveness at high wind speeds (>10.7 m/s), highlighting the need for additional containment strategies. Future research should explore long-term durability, ecological impact, and cost-effectiveness of large-scale deployment.

1. Introduction

Water, the most vital resource on Earth, is increasingly scarce due to ongoing population growth and the impacts of climate change (El-Ghannam et al., 2021; Li et al., 2021). As a key tool for climate change adaptation, the construction of dams and reservoirs can help mitigate the adverse impacts of climate extremes—such as floods and droughts—on already limited water resources (Lehmann et al., 2019; Rocha et al., 2020). In arid and semi-arid regions, plain reservoirs play a crucial role in managing limited surface runoff for agricultural irrigation, as well as domestic and industrial water use (Althoff et al., 2020a, 2020b). While reservoir construction is vital for supporting agricultural

development in these areas, it also brings negative effects, such as significant evaporation from reservoirs in arid zones. Reservoirs in Texas, USA, experience evaporation losses of around 40 %-60 % (Friedrich et al., 2018), while Lake Nasser in Egypt has an evaporation loss of about 20 % (El-Shirbeny and Abutaleb, 2018), and reservoirs in Queensland, Australia, lose approximately 40 % to evaporation (Craig et al., 2005). In Xinjiang, China, evaporation accounts for more than 40 % of the total water storage (Han et al., 2020). This significant evaporation exacerbates water scarcity in arid regions and increases the salt concentration in reservoir water due to evaporation concentration.

A well-recognized issue with plain reservoirs is the gradual salinization of the water stored within them, which significantly limits their

* Correspondence to: College of Hydraulic and Civil Engineering, Xinjiang Agricultural University, No. 311 Nongda East Road, Shayibake District, Urumqi 830052, China.

E-mail addresses: 465711021@qq.com (G.-c. Hao), xndsg@sina.cn (K.-B. Shi), 595607123@qq.com (K.-w. Han).

<https://doi.org/10.1016/j.agwat.2025.109440>

Received 25 December 2024; Received in revised form 2 March 2025; Accepted 14 March 2025

Available online 28 March 2025

0378-3774/© 2025 Published by Elsevier B.V. This is an open access article under the CC BY-NC-ND license (<http://creativecommons.org/licenses/by-nc-nd/4.0/>).

effective functioning. In irrigated areas with flooded soils, the use of highly saline water from these reservoirs for irrigation is a major cause of land salinization (Gebrehiwet et al., 2021). Excessive evaporation and bottom leakage from arid plain reservoirs release highly saline water, which raises local groundwater levels and increases the risk of soil salinization in irrigated agricultural areas near and downstream of the reservoirs (Peng et al., 2007; Grünberger et al., 2008; Cui and Shao, 2005). It is estimated that 33 % of the world's irrigated land and 20 % of cultivated croplands are affected by high salinity (Shrivastava and Kumar, 2015). According to (Zaman et al., 2018) in their publication Guideline for Salinity Assessment, Mitigation, and Adaptation Using Nuclear and Related Techniques, 20 % of India's arable land is impacted by salinity, and 10 million hectares of land in Pakistan are affected by soil salinity. In Northwest China, the saline-alkali area exceeds 2 million hectares, representing about one-third of the country's total saline-alkali land (Yuan et al., 2018). Additionally, for various reasons, the global land area affected by salinization is increasing at a rate of 10 % per year (Shrivastava and Kumar, 2015).

In arid and semi-arid regions, the risk of soil salinization caused by the export of highly saline water from plain reservoirs has become a significant issue (Gassama et al., 2012; Hammecker et al., 2012). Therefore, finding ways to prevent the salinization of reservoir waters is crucial for the efficient use of water resources and for improving the ecological environment in arid zones.

Most previous studies have focused on initial salinity control in new reservoirs, including methods such as excavating alkali drainage ditches before impoundment, disturbing sediments to promote salt release, discharging highly saline water, using plants for salt uptake, and reducing salt release fluxes at the water-soil interface by decreasing the size of the reservoir (Fan et al., 2022). In addition, controlling nutrient inputs from upstream water sources, implementing ecological restoration of reservoir ecosystems, removing highly saline soils from the surface layers of reservoirs, and enhancing the structure and function of aquatic ecosystems can further reduce the risk of eutrophication in newly built reservoirs (Zhu et al., 2015). However, most of the studies mentioned above have focused on newly constructed reservoirs, with fewer exploratory studies addressing the long-term inhibition of water salinization during the operation and maturation phases.

Research on the salinization mechanisms of reservoirs and lakes indicates that the main factors affecting water salinization include: (1) the concentration of salts due to water evaporation, (2) the acceleration of salt dissolution in reservoir sediments caused by wind and wave disturbances, and (3) the discharge of highly saline water from adjacent aquifers through underwater springs or seepage zones (Mongelli et al., 2013; Cary et al., 2015; Merchán et al., 2015). Controlling the factors mentioned above can help alleviate water salinization. The findings of (Zhu et al., 2015) showed that the release of salt from sediment was the primary cause of early salinization in reservoir water. Over time, however, the salinization due to evaporation and concentration became increasingly prominent. Studies by several researchers have shown that inhibiting evaporation by covering water bodies with anti-evaporation materials can help reduce salt concentrations. For example, (Maestre-Valero et al., 2011) investigated the effect of covering a 2400 m² irrigated agricultural reservoir with sunshade nets and found that the inhibition of evaporation led to an 8.2 % reduction in conductivity.

Regarding the selection of anti-evaporation materials, common covers such as shade nets, vinyl foam discs, and chemical polymer film covers are susceptible to breakage, stacking, and loss of coverage area in windy conditions typical of arid zones. This results in a reduction in their anti-evaporation effectiveness, with performance dropping by approximately 30–60 % (Aminzadeh et al., 2018; Mady et al., 2021; Abdallah et al., 2021). In contrast, high-density polyethylene floating spheres, due to their curved structure, are less likely to stack or be displaced by wind. These spheres offer a high anti-evaporation efficiency (over 75 % when the water surface is fully covered) and have become one of the most

commonly used anti-evaporation cover elements in recent years (Abdallah et al., 2021; Han et al., 2020).

Hao et al. (2023) used floating spheres as an anti-evaporation material in an evaporator with a diameter of 1.2 m to study the water quality of a water body at 74.98 % coverage. The results indicated that the water conductivity value was reduced by 46.59 %. However, floating spheres have not been widely tested in large reservoirs, necessitating further research. Therefore, it was hypothesized that floating HDPE spheres would significantly reduce evaporation and salinity levels in reservoirs by inhibiting evaporation from the water column and preventing sediment resuspension. The objectives of this study were: 1) to quantify the effect of floating spheres on evaporation, 2) to analyze changes in salinity levels under different wind-dynamic conditions, and 3) to assess the impact of floating spheres on water chemistry, including pH and dissolved oxygen.

In the actual operation of the reservoir, the floating spheres are easily dispersed by the wind and cannot be tightly arranged without assistance. To address this, a floating box fence (40 × 40 × 50 cm) made of the same black high-density polyethylene (HDPE) material was used to gather the floating spheres, ensuring an effective coverage area for evaporation control.

At the same time, based on the water-salt balance and considering both the water volume in the reservoir and its existing salt content, the study combined the salt concentration of the reservoir water under the floating sphere cover at the field site with evaporation tests and water chemistry parameter tests to assess the impact of salt release from the water body. The aim of this study is to investigate the salt release pattern and the spatial and temporal distribution of bottom sediments under the cover of the anti-evaporation floating spheres, as well as to quantify the impact of evaporation inhibition on salt concentration. This research will provide valuable insights for controlling the salinization of reservoir water over extended time periods.

2. Materials and methods

2.1. Experimental area

This study was conducted at the Shengjintai Reservoir in the Heigou Basin, located in Turpan, Xinjiang, China. The Heigou Basin is characterized by a mountainous and hilly landscape, with elevations ranging from 110 m to 156 m, and has a typical continental warm-zone arid desert climate. The reservoir's catchment area covers 31.6×10^4 m², with a total capacity of 118.6×10^4 m³. It is classified as a small (I) type of diversion reservoir, primarily used for agricultural irrigation. See Fig. 1. Due to drought, wind erosion, sandstorms, and frequent human activities, land desertification is progressing rapidly in the basin. Soil erosion is severe, and the irrational use of land and water resources has led to a gradual increase in the salinity of the region's water bodies. The region features a low hilly landscape with an average altitude of 150 m and a typical continental warm-belt arid desert climate. The multi-year average annual temperature is 15.7°C, with a maximum of 47.7°C and a minimum of -25.2°C. The average relative humidity ranges from 14 % to 25 %, while the annual wind speed averages 1.5 m/s, with maximum wind speeds reaching up to 25 m/s. The average annual precipitation is 16.2 mm, with a maximum of 48.4 mm, while the potential evaporation in the reservoir area is 1509.0 mm. The ratio of annual precipitation to potential evaporation is less than 0.05, classifying the region as an extreme arid zone according to the Food and Agriculture Organization of the United Nations (Spinoni et al., 2013). The meteorological parameters of the study area are shown in Fig. 2.

2.2. Experimental design

In this experimental study, a combination of laboratory and field tests was employed to investigate the impact of the floating sphere cover on the spatial and temporal distribution of salinity in the reservoir

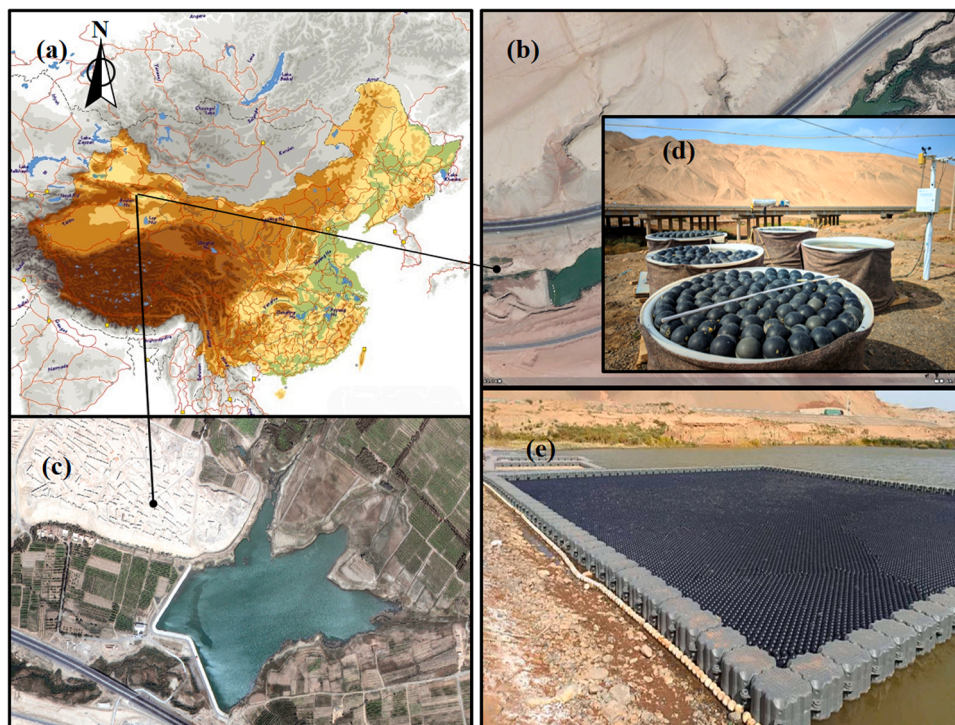


Fig. 1. Geographical location of the test site, in which (a) the geographical location of Shengjintai Reservoir in Turpan, Xinjiang, China, (b) the downstream pond dam of Shengjintai Reservoir, (c) Shengjintai Reservoir, (d) the downstream pond dam is paved with 400 m² floating spheres, and the floating spheres are centrally fixed by floating boxes, (e) five groups of evaporators with different coverage rates are paved with weather stations and near Shengjintai Reservoir Dam, and bottom mud deposits are laid in the evaporators.

water. Substrate samples were collected from the surface (0–15 cm) of the beach area during the dry season. The sediments were initially sieved using a 10 mm mesh to remove boulders, weeds, debris, and other impurities before being placed at the bottom of the outdoor evaporator. Five sets of evaporators, each with a height of 0.8 m and a diameter of 1.2 m, were used in the study.

The indoor test samples were further sieved and sealed using a 1 mm mesh. Additionally, water samples were collected from the 1.2 m evaporator under different seasonal conditions, as well as from the reservoir site under varying wind speeds, to monitor water quality parameters such as salinity, suspended solids concentration, dissolved oxygen, and pH.

2.2.1. Indoor experiments

The collected substrate samples were spread in a 1500 ml beaker to a thickness of 2 cm, and deionized water was slowly added along the wall of the beaker until the water level reached 8 cm. Four parallel test groups were set up and placed in a constant-temperature incubator. The water temperature (T), dissolved oxygen (DO), and pH were adjusted to match the measured environmental conditions at the reservoir site. Using the control variable method, a single aquatic environmental factor was adjusted at a time. Water temperature (T) was regulated using a constant temperature incubator, pH levels were adjusted with HCl and NaOH solutions, and dissolved oxygen (DO) was modified by introducing nitrogen (N₂) or oxygen (O₂) into the water. If the dissolved oxygen levels could not be precisely maintained at the set value, the actual measured values were used, ensuring they were as close as possible to the target levels. The four test groups were left to stand for 15 days and 50 ml of water samples from the intermediate water column were taken at 24-hour intervals and replenished to the original water level to calculate the flux of release of salts from the bottom sediment to the overlying water under different environmental conditions. Dissolved oxygen concentration (DO) and water conductivity values were determined using water quality testing instruments. Water-suspended solids

(SC) were determined using the filter weighing method. Before each reading, ensure that no residual impurities remain on the sensor's surface. Immerse the sensor in a calibration solution of known concentration, then record the calibration value and calibrate the sensor to ensure measurement accuracy before taking the reading.

2.2.2. Reservoir field trials

Five identical evaporators (diameter 1.2 m, height 0.8 m) made of high-density polyethylene (HDPE) were positioned on top of the reservoir dam. The bottoms of the evaporators were covered with a 15 cm layer of bottom sediment. Black HDPE floating spheres (diameter 0.1 m, thickness 2 mm, weight 50 g) were placed in each evaporator as an anti-evaporation material. To prevent heat exchange between the water and the surrounding environment through the side walls, the outer walls of the evaporators were insulated with cotton. To facilitate the comparison between the covered area and the corresponding evaporation in an evaporator with a diameter of 1.2 m, the water surface of the evaporator was divided into four equal sections. The number of floating spheres used in the five evaporators was 0, 27, 54, 81, and 108, corresponding to coverage areas of 0%, 18.74%, 37.49%, 56.23%, and 74.98%, respectively. In the actual laying of the reservoir, the true area of coverage should be calculated according to the number of floating spheres laid. The area covered by the floating spheres was controlled using a removable PVC baffle. To account for the effect of evaporator size on evaporation, a standard evaporator with a diameter of 20 cm was installed in an open area, where it receives direct sunlight throughout the day, serving as a reference. A fence made of a floating box with dimensions 50 cm × 50 cm × 40 cm was placed in the pond dam downstream of the reservoir to gather the high-density polyethylene floating spheres, ensuring that the points between the spheres are closely connected. The test setup is shown in Fig. 1(d) and (e).

2.2.3. Meteorological and evaporation data collection

Daily evaporation for the standard 20 cm diameter evaporator was

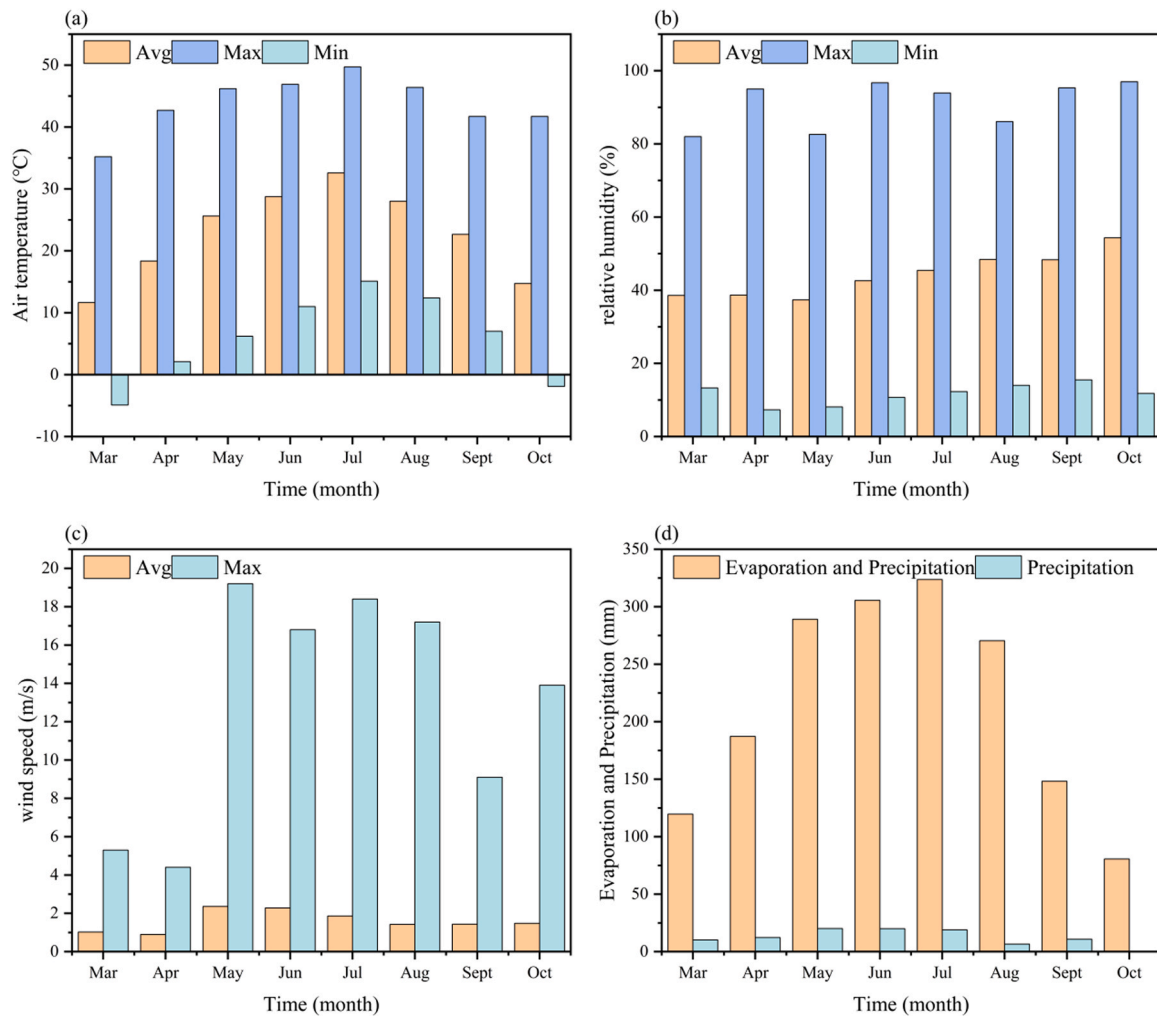


Fig. 2. Meteorological parameters of the study area, in which (a) is monthly average temperature (b) monthly average relative humidity (c) monthly average wind speed (d) monthly average evaporation and rainfall.

measured using the weighing method, while evaporation for the 1.2 m diameter evaporator was recorded using a water level stylus (model LD-SCM40; accuracy ± 0.1 mm). Precipitation data were collected using a rain gauge (model RS-05B; accuracy ± 0.1 mm), with measurements taken after each rainfall event. Water lost to evaporation was replenished to the original water level every 7 days. To avoid the influence of temperature differences in the newly added water on the evaporation data, the water temperature and evaporation data from the day following water replenishment were excluded. This study only monitored meteorological data related to the non-freezing period (March to October) and evaporator evapotranspiration. The freezing period was not monitored because evapotranspiration during the colder months accounted for only 5.3 % of the annual total, and the evaporator at the field site was often iced over, making it difficult to collect accurate evapotranspiration data. A mobile weather station (Model: NK5500) was set up in the open area near the evaporator, where it automatically recorded atmospheric temperature, humidity, wind speed, and other meteorological data every 10 minutes. Additionally, water temperature sensors (Model: FR-WTS, accuracy: $\pm 0.5^\circ\text{C}$) were installed at various depths below the water surface: 10 cm, 20 cm, 30 cm, 40 cm, 50 cm, and 60 cm. The water temperatures were recorded from top to bottom as T0w, T1w, T2w, T3w, and so on. To ensure accurate surface temperature readings, the sensor for monitoring water surface temperature was positioned 1 cm below the surface to prevent detachment due to fluctuations in water level. Temperature sensors were installed on the

surface of the floating spheres to monitor surface temperature, with data recorded every 2 hours. Additionally, temperature and humidity sensors (Model: RS485, accuracy: $\pm 0.5^\circ\text{C}$, ± 0.2 % RH) were placed above the evaporator water surface to record temperature and humidity fluctuations at various coverage rates, with measurements taken every 10 minutes.

2.3. Research methodology

Electrical conductivity (EC) measures the ability of a solution to conduct an electric current and, in the case of water, is often used to estimate the total concentration of dissolved salts. Since aqueous conductivity is temperature-dependent, we normalized the collected EC data to 25°C to account for this variation, following the procedure outlined in Eq. (1) (Hayashi, 2004).

$$Ec_t = Ec_{25}[1 + a(t - 25)] \quad (1)$$

Where Ec_t is the conductivity at temperature t ($^\circ\text{C}$), Ec_{25} is the conductivity at 25°C , and a is a temperature compensation factor, which is 0.0187 here.

The total salt content in the overlying water at a given time can be determined from the conductivity-salt concentration plot and the volume of the water body. By subtracting the total salt content in the overlying water at time t_i from that at t_{i-1} , the total salt released from the bottom sediment to the overlying water during the period can be

calculated. The flux of salt released from the subsoil sediments to the overlying water is then expressed as the ratio of total salt released to the time interval and the area of the water-soil interface, as shown in Eq. (2).

$$flux_i = \frac{\Delta m_i}{\Delta t_i \times A} \quad (2)$$

Where: $flux_i$ is the salt flux at the water-soil interface at the i th moment ($g/(cm^2 \cdot h)$); Δm_i is the increase in salt in the water column at the i th moment (g); Δt_i is the time interval chosen for the i th calculation moment; and A is the area of the sediment-water interface (cm^2);

For the 1.2 m diameter evaporator in a water body without seepage or groundwater exchange, the increase in salt concentration in the water is primarily due to evaporation and concentration, as well as the release of salts from the bottom sediment into the overlying water. The contribution of evaporation and concentration, as well as the release of salts from the bottom sediment to the overlying water, to the increase in salt concentration, can be expressed by formulas (3) and (4):

$$P_e = \frac{\Delta C_e}{\Delta C} \quad (3)$$

$$P_f = \frac{\Delta C - \Delta C_e}{\Delta C} \quad (4)$$

Where: P_e is the average contribution to the increase in conductivity of the water body by evaporative concentration; P_f is the average contribution to the increase in conductivity of the water body by the release of salts from the bottom sediment to the overlying water body; ΔC_e is the amount of increase in conductivity of the water body caused by evaporative concentration ($\mu s/cm$); and ΔC is the total amount of increase in conductivity of the water body over the period ($\mu s/cm$).

where ΔC_e can be calculated by the following equation:

$$\Delta C_e = C_{ti(i-1)} - C_{ti} = C_{ti}(V_{ti}/V_{ti(i-1)} - 1) \quad (5)$$

Where C_{ti} is the conductivity of the water body at the moment of t_i ; V_{ti} is the volume of the water body at the moment of t_i ; $C_{ti(i-1)}$ is the conductivity of the water body at the moment of $t_{(i-1)}$; and $V_{ti(i-1)}$ is the volume of the water body at the moment of $t_{(i-1)}$. When replenishment starts in the evaporator, the conductivity of the water body after replenishment is used as the initial conductivity of that water body. The salt diffusion flux in a 1.2 m diameter evaporator and the average contribution of water body evaporation and salt concentration diffusion to the conductivity of the water body at different coverage rates were calculated from field experiments.

Using the uncovered evaporator as a blank control group, after a period of water surface evaporation, the evaporation from the water body in the uncovered group was E and the water body salt concentration was S . The evaporation from the water surface in the covered group was E_c and the water body salt concentration was S_c can be obtained:

Evaporation inhibition rate formula:

$$\varepsilon_e = 1 - E_c/E \quad (6)$$

Salt concentration reduction rate calculation formula:

$$\varepsilon_s = 1 - S_c/S \quad (7)$$

Water balance modelling:

$$V_1 + R + P = O + G + E + V_2 \quad (8)$$

In the formula, V_1 represents the water volume in the reservoir at the start of the calculation period (m^3); R is the volume of water flowing into the reservoir (m^3); P is the precipitation volume (m^3); O is the volume of water flowing out of the reservoir (m^3); G is the leakage from the reservoir (with $G = 0$ for a closed container) (m^3); E is the water lost due to evaporation from the reservoir (m^3); and V_2 is the water volume in the reservoir at the end of the calculation period (m^3).

Salt balance model:

$$V_1 S_V + R S_R = O S_O + G S_G + (E + V_2 - P) S \quad (9)$$

Where S_V is the original mineralisation of the reservoir water, g/L ; S_R is the average mineralisation of the inflow water to the reservoir, g/L ; S_O is the average mineralisation of the outflow water from the reservoir, g/L ; S_G is the average mineralisation of the seepage water from the reservoir, g/L ; and S is the average mineralisation of the water in the reservoir at the end of the calculation period, g/L .

2.4. Statistical analyses

After processing the data using Excel software, IBM SPSS Statistics 22 was used to perform curve fitting between the salt release fluxes and water conductivity data. Confidence intervals were calculated, and for water conductivity, three samples were taken at a time. Statistical tests were conducted to calculate the probability (p-value) that the differences between the samples were due to sampling error. Tukey's test was then used to analyze the differences in water conductivity and turbidity between the floating sphere-covered and uncovered groups, as well as the correlations ($p \leq 0.05$) between wind speed and water turbidity, and wind speed and water conductivity under no coverage conditions.

3. Results

3.1. Correlation between conductivity and salt content

Direct monitoring of water salinity at the reservoir site is difficult. However, existing studies show that water salinity is linearly related to conductivity, which can be used to estimate salinity in aqueous solutions. Monitoring conductivity is simpler and more practical, and the relationship between conductivity and salinity allows conductivity to effectively reflect changes in the salt concentration of the water column.

The substrate samples were dissolved in varying volumes of distilled water, and the conductivity and salinity of each solution were analyzed to establish the correlation between water conductivity and salinity, as shown in Fig. 3. The results demonstrated a linear relationship, expressed by the equation $y = a + bx$, with a correlation coefficient of $R^2 = 0.931$. Thus, changes in water conductivity can be used to track the pattern of salinity variation in the water body.

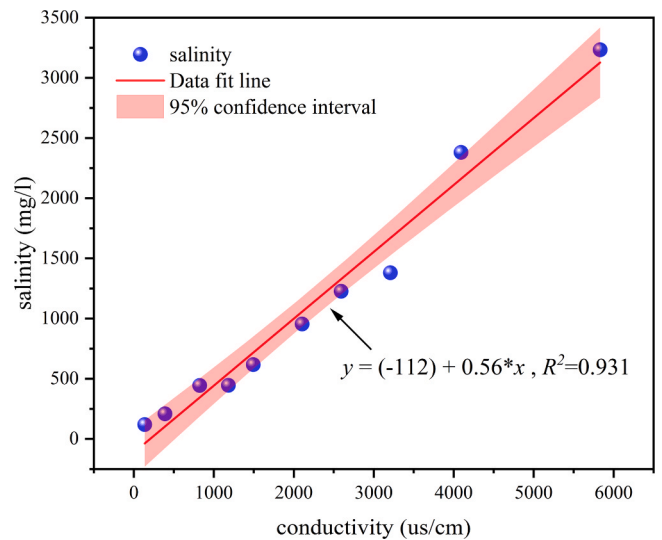


Fig. 3. Relationship between conductivity and salt content, Each data set is the mean of 3 measurements, and the p-value for each sample measurement is ≤ 0.05 .

3.2. Calculation of salt release fluxes from bottom sediments

3.2.1. Changes in conductivity of overlying water

In March, at the beginning of the experiment, a 15 cm layer of reservoir bottom sediment was placed in the evaporator to investigate the salt release pattern from the sediment to the overlying water. Changes in salt concentration in the water column were monitored 30 days after laying the bottom sediment, and the salt release flux was calculated. Based on salt and water balance equations, the increase in salt concentration in the evaporator was attributed to both the release of salts from the substrate sediment and the evaporation and concentration of the water body. Since there was no sand or dust in March, the effect of air deposition on salt concentration was negligible. Water samples were collected from the upper, middle, and lower layers (20 cm, 40 cm, and 60 cm) of the evaporator, and the average conductivity of each layer was used to represent the conductivity of the water during that period. The change in conductivity of the upper layer of water is shown in Fig. 4.

From the fitted curves in Fig. 4, which depict changes in overlying water conductivity and the rate of conductivity increase, it is evident that the salt concentration in the overlying water follows an exponential growth pattern. Initially, during the first two days, the conductivity of the overlying water increases sharply by 147%. However, this rate of increase declines rapidly over time as the release of salt from the substrate to the overlying water gradually diminishes. By approximately the 10th day, the rate of conductivity increase stabilizes.

3.2.2. Salt release from the substrate at the beginning of water intake

The increase in salt concentration in the evaporator results from two factors: the release of salt from the bottom sediment and the evaporation and concentration effect. Using the formula $C_1V_1 = C_2V_2$, the increase in salt concentration due to evaporation can be calculated on a daily basis. During the one-month monitoring period, no dusty weather occurred, so after excluding the effects of dust, the total increase in conductivity concentration, minus the increase caused by evaporation, represents the increase in salt concentration in the overlying water due to salt release from the bottom sediment. The contribution of evaporation and substrate salt release to the overall increase in salt concentration over one month is shown in Fig. 5(b).

Conductivity values were averaged based on the conductivity of the water column in the evaporator, accounting for the gradual decrease in the rate of salt release from the bottom sediment to the overlying water over time. Data collection occurred every 2 hours on the first day, every 6 hours on the second day, and once daily at 8 p.m. thereafter, with the average conductivity of the water column in the evaporator representing

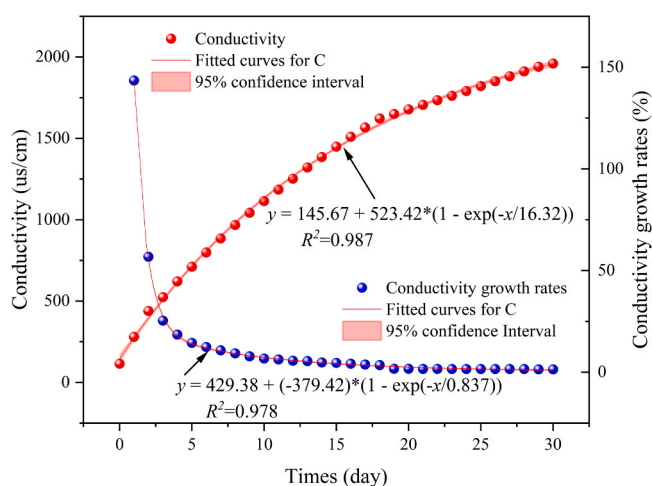


Fig. 4. Electrical conductivity and growth rate of overlying water, Each data set is the mean of 3 measurements, and the p-value for each sample measurement is ≤ 0.05 .

the value for each day.

The salt release flux from the sediment in the evaporator at each time point was calculated using Eq. 1, and the variation of this salt flux over time is shown in Fig. 5. The results indicate that the salt release flux gradually decreases as time progresses, with the data distribution following a negative power exponential function. As shown in Fig. 5, during the initial phase of subsoil placement, the majority of salt release occurred within the first 96 hours, with the most significant release happening in the first 6 hours. After the 10th day, the salt release from the water-soil interface stabilized. By day 19, as the surface subsoil salt content decreased and the salt concentration in the overlying water increased, the salt gradient between the water and sediment diminished. As a result, in the quiescent water column, the salt release from the subsoil to the upper overlying water weakened significantly, reaching a low rate of only $310 \text{ mg}/(\text{m}^2\cdot\text{h})$.

The increase in salinity of the overlying water during the first 15 days was primarily attributed to salt release from the sediment, with the cumulative contribution from sediment accounting for 93.38% of the increase in salinity. After day 15, the rise in salt concentration in the water body was mainly driven by evaporation and concentration. By this point, evaporation contributed 77.19% to the overall increase in salinity. In fact, around day 20, the contribution from sediment became negative, likely due to the adsorption of nitrogen and phosphorus nutrients from the sediment into the water, which counteracted the salinity increase.

3.3. Contribution of salt growth on a monthly scale

3.3.1. Effect of inhibited evaporation on salt concentration

From March to October, the conductivity of the water column in each evaporator was monitored separately over a complete irrigation cycle, with varying coverage rates, to assess the impact of floating sphere coverage on salt concentration. Due to the small size of the evaporators, there was no noticeable difference in conductivity values between the covered and uncovered areas within the same evaporator, so the average conductivity of the entire water column was used. The monthly increase in conductivity values for each coverage rate is shown in Fig. 6(a), while the conductivity reduction is depicted in Fig. 6(b).

As shown in Fig. 6, the increase in conductivity values in the water body is positively correlated with evaporation. In July, when temperatures were highest, the conductivity value of the uncovered group reached $1720 \text{ }\mu\text{S}/\text{cm}$. However, when the evaporator surface was covered with 74.98% floating spheres, the conductivity value decreased by 59.03%. Over the course of a complete irrigation cycle (March to October), the average reduction in conductivity values for the covered groups (with 18.74–74.98% coverage) compared to the uncovered group ranged from 10.30% to 46.9%.

3.3.2. Potential contribution of bottom sediments and evaporation to salinity increase

To closely simulate substrate releases at the reservoir site, the evaporator substrate was not replaced during the test period from March to October; only the water lost to evaporation was replenished. By monitoring both evaporation and the conductivity of the overlying water, the incremental increase in conductivity values was calculated. This allowed for the separate calculation of the contributions from the substrate and evaporation to the increase in salinity concentration of the overlying water for each month, as shown in Fig. 7.

As shown in Fig. 7(a), the annual average evaporation inhibition rate of the 1.2 m diameter evaporator ranges from 13.56% to 60.19% when the water surface is covered with floating spheres at coverage rates between 18.74% and 74.98%. This demonstrates a significant evaporation suppression effect. The contributions of the substrate and water evaporation to the salt concentration in the water column under varying seasonal conditions can be determined by monitoring both the evaporation rates and the conductivity of the overlying water. As shown in

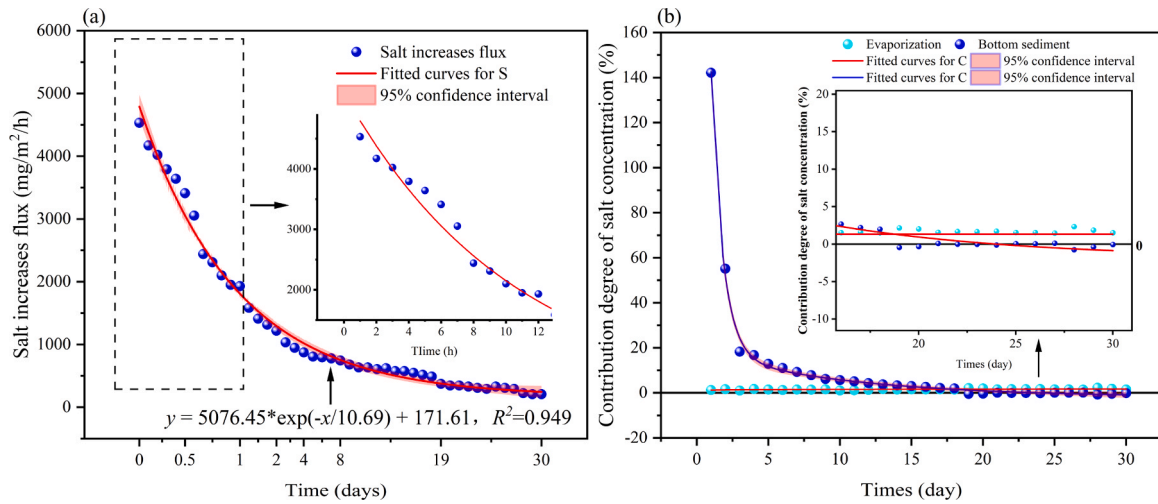


Fig. 5. (a) Salt release flux, (b) Contribution of sediment release and evaporation rate concentration to the increase of salt concentration, Each data set is the mean of 3 measurements, and the p-value for each sample measurement is ≤ 0.05 .

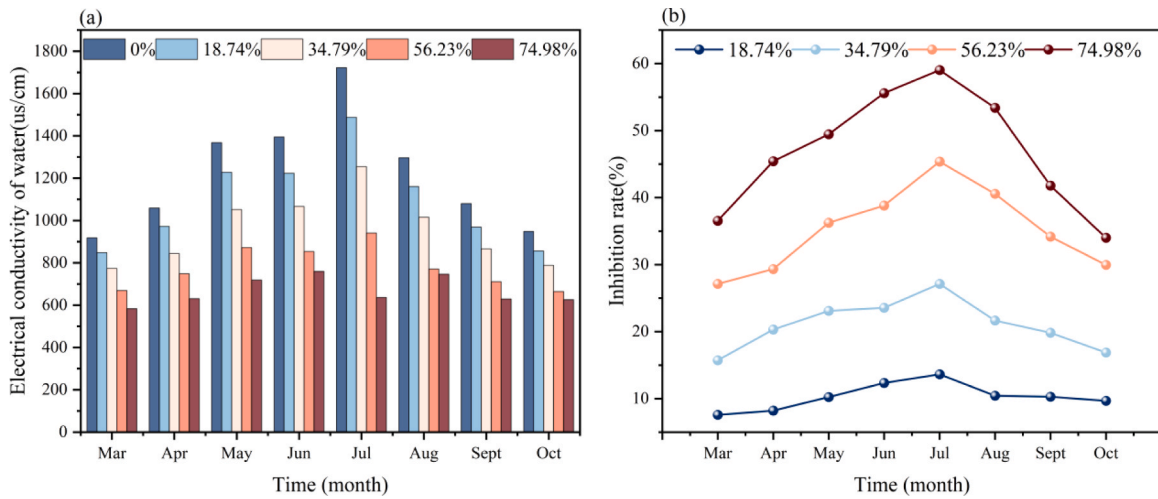


Fig. 6. (a) Water conductivity in evaporators with various coverage rates on a monthly scale, and (b) Inhibitory effect of floating sphere covering on conductivity increment.

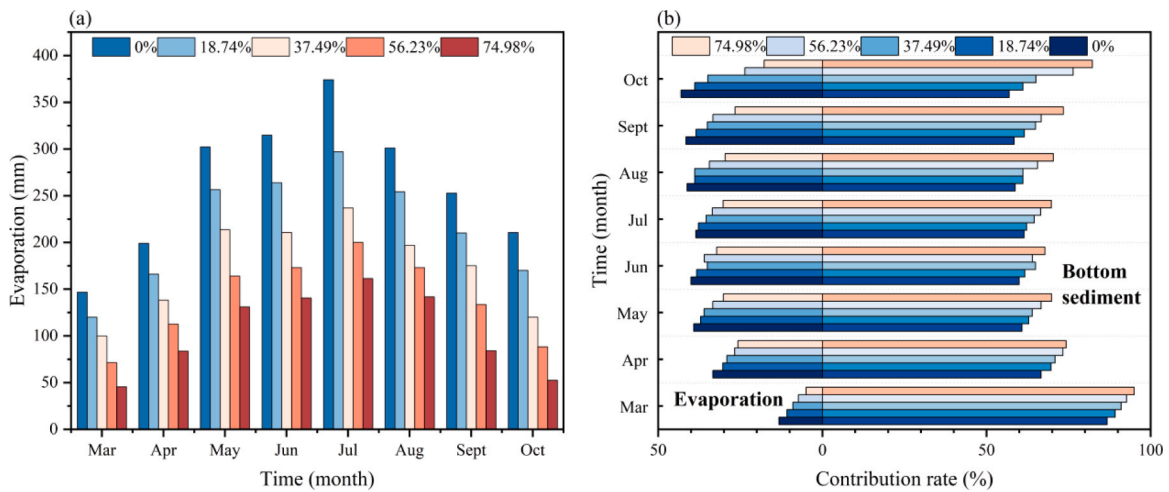


Fig. 7. (a) monthly scale evaporation of 1.2 m evaporator with different coverage, (b) contribution rate of sediment salt release (right) and evaporation (left) to the increase of salt concentration.

Fig. 7(b), at the start of the subsoil placement in March, the increase in overlying water salinity concentration in the uncovered group due to the release of salts from the substrate was as high as 86.7 %. However, as the salts were gradually released from the surface subsoil sediments, the contribution of the subsoil to the increase in overlying water salinity concentration decreased. By October, the contribution from the subsoil had dropped to 56.95 %.

Throughout the entire test cycle, the contribution to the increase in water column salinity due to evaporation ranged from 36.28 % to 24.65 % for evaporators with 0–74.98 % coverage. In contrast, the contribution from the substrate ranged from 63.71 % to 75.34 %. As the water surface was covered with 18.74 %–74.98 % floating spheres, the salt concentration caused by evaporation decreased by 6.8 %, 12.71 %, 21.38 %, and 32.09 %, respectively.

3.4. Impact of floating spheres covering the water surface on water quality parameters

The shading effect of water surface coverings that inhibit evaporation, along with the impact of heat transfer to the water column, can influence water quality and the overall water environment, potentially altering salt transport within the water column. Therefore, a combination of (1) the effects of the cover on water quality parameters in evaporator-covered water bodies in a field setting and (2) the impact of water quality parameters on salt release in the experimental chamber was used to analyze the salt migration patterns in the water column after the water surface was covered with anti-evaporation floating spheres.

3.4.1. Effects on water temperature

Studies have shown that covering the water surface with anti-evaporation floating spheres impacts water temperature. The effect of floating sphere coverage on water temperature can be observed by statistically analyzing a stationary water body with varying coverage levels during the non-freezing period. The water body was divided into three layers (approximately 20 cm each), and the temperature distribution at different depths was monitored in each experimental group, as illustrated in Fig. 8. The fluxes of salt release from the bottom sediment under different temperature conditions are shown in Fig. sf1 of the supporting document.

When the water surface was covered with 18.74–74.98 % floating spheres, the average temperature of the upper water layer increased by 0.29–1.74 °C, while the middle water layer's temperature decreased by 0.45–0.16 °C, and the bottom water layer's temperature dropped by 0.6–1.21 °C compared to the uncovered control group. Overall, the

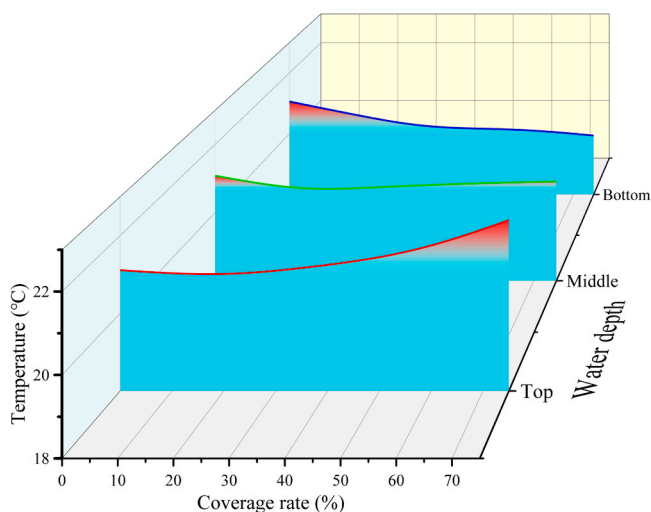


Fig. 8. Shows the average temperature between water bodies with different water layers.

floating sphere coverage reduced the average water temperature by 0.25–0.63 °C. According to the supporting document Fig. sf1, the increase in temperature enhanced the release of salts from the bottom sediment, with the release flux being directly proportional to the temperature, both at the start of the experiment and 10 days after the salt release had stabilized. The shading effect of the floating spheres significantly cooled the bottom water layer, which in turn lowered the temperature of the upper water body and the bottom sediment. This temperature reduction helped to inhibit the salt release from the sediment.

3.4.2. Effect of floating sphere coverage on dissolved oxygen

The dissolved oxygen (DO) content of the water column in the evaporator, with varying coverages across different months, as well as the flux of salt release from the bottom sediment to the overlying water under different DO conditions in the test chamber, were monitored and are shown in Fig. 9. Release fluxes of salts from the substrate to the overlying water column at different dissolved oxygen levels are shown in Fig. sf2 of the Supporting document.

The DO content in the water column decreased as the temperature increased, exhibiting a clear seasonal pattern throughout the test period. In static water bodies with 18.74 %, 34.79 %, 56.23 %, and 74.98 % coverage, the dissolved oxygen concentration decreased by 1.21 %, 3.45 %, 6.41 %, and 8.54 %, respectively. Based on Fig. sf2 of the Supporting document, within a specific range of dissolved oxygen levels, the salt released from the sediment is negatively correlated with the dissolved oxygen content in the water body ($DO=2 > DO=5 > DO=7 > DO=9$). As the experimental period progresses, the increase in salt concentration in the overlying water gradually decreases and stabilizes by the 5th day.

3.4.3. Effect of floating sphere coverage on the pH of water bodies

PH is a crucial water quality parameter that influences the migration of soluble nitrogen and phosphorus nutrients from the bottom sediment into the water column. The PH levels of the water body in the evaporator were monitored for each coverage rate. Four different water environments with pH values of 5, 7, 8, and 10 were established for a 15-day salt release test. During the test, the electrical conductivity of the substrate overlying water was monitored, and the salt release fluxes from the sediment to the overlying water were calculated for each pH condition. Release fluxes of salts from the substrate to the overlying water column at different pH values support document Fig. sf3.

The monitoring results revealed that the pH of the water body in the reservoir area from March to October ranged between 7.8 and 8.6,

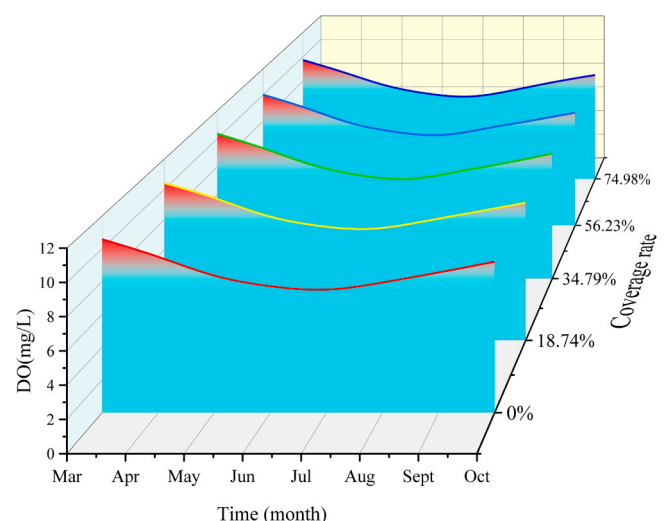


Fig. 9. Dissolved oxygen in evaporator water with different coverage.

indicating a weakly alkaline water body. Floating sphere coverage had a minimal impact on the water pH. When the water surface was covered with 18.74 %, 34.79 %, 56.23 %, and 74.98 % floating spheres, the average pH value of the water was reduced by only 0.75 %, 1.21 %, 2.27 %, and 3.18 %, respectively, as shown in Fig. 10. Floating sphere coverage on the water surface reduced the pH, but the water remained weakly alkaline across all coverage groups and was only minimally affected. The lowest pH value in the evaporator, occurring with the maximum surface coverage (74.98 %), was 7.5 in March. In-house results indicated that the intensity of salt release from the bottom sediment was highest under alkaline conditions ($\text{pH} = 10 > \text{pH} = 8$), followed by acidic ($\text{pH} = 5$), and lowest under neutral conditions ($\text{pH} = 7$). Therefore, while the floating sphere coverage helped inhibit evaporation from the water column, it only slightly attenuated salt release from the bottom sediment.

3.5. Inhibition of re-suspension of bottom sediment by floating sphere cover

Wind speed data collected from the test area revealed that the maximum wind speed at 2 m above the surface during the entire test cycle was 19.2 m/s. Since the water intake in the test reservoir remained relatively consistent from May to June, with only slight fluctuations in the water level, water samples were collected from the reservoir area under varying wind speed conditions during these months.

The wind speed data collected on specific dates, such as June 17th, May 27th, June 10th, May 23rd, June 14th, May 31st, June 2nd, and May 21st, correspond to different wind levels: Level I (light air, 0.3–1.5 m/s), Level II (light breeze, 1.6–3.3 m/s), Level III (gentle breeze, 3.4–5.4 m/s), Level IV (moderate breeze, 5.5–7.9 m/s), Level V (fresh breeze, 8–10.7 m/s), and Level VI (strong breeze, 10.8–13.8 m/s). The wind dynamics throughout the test period ranged from Level II to Level VIII, including conditions such as moderate gale (13.9–17.1 m/s) and fresh gale (17.2–20.7 m/s). The daily maximum and average wind speeds at the reservoir site during the entire test cycle are presented in Fig. 11.

3.5.1. Distribution characteristics of turbidity and conductivity in the water column under different wind and wave disturbances

Most plain reservoirs in arid zones have shallow water depths, making the bottom sediments prone to re-suspension by wind and waves. This causes the salts in the deeper sediments to diffuse into the overlying water. To mitigate this, we placed 400 m² of floating spheres at the downstream pond dam, as shown in Fig. 1(d). From May to July,

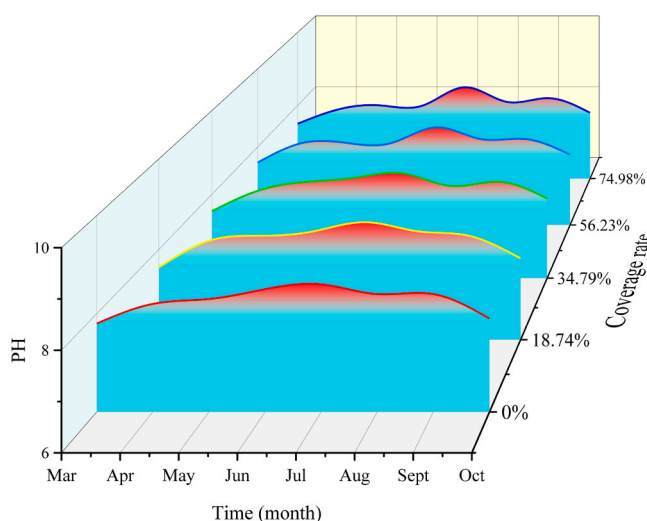


Fig. 10. PH value of evaporator water body under different coverage rates.

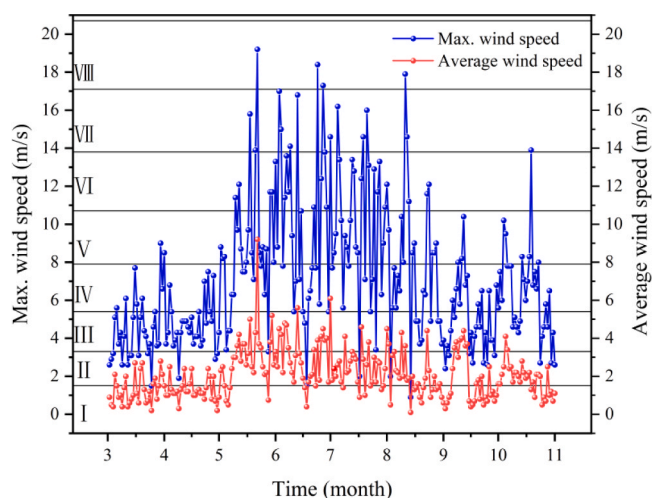


Fig. 11. Distribution of Maximum and Average Wind Speed in Reservoir Site.

two sampling points were established in both the covered and uncovered areas of the floating spheres. A small water pump, connected to a hose attached to a straight rod with a scale, was used to collect samples at designated depths. Stratified sampling was employed to obtain water samples from different depths at the sampling points, under varying wind-dynamic conditions. The concentration of suspended solids and electrical conductivity values of the water samples were then measured. The floating sphere cover was employed to analyze the re-suspension and salt release from the bottom sediment under varying wind speeds. Fig. 12 illustrates the vertical distribution of suspended sediment concentration and conductivity at different water depths and wind speeds, while Fig. 13 shows the inhibition rate of suspended sediment content in the water column due to the floating sphere cover at different wind speeds.

As shown in Figs. 12 and 13, when the wind speed increased from Class I (1.5 m/s) to Class VIII (19.2 m/s), the concentration of suspended solids in the substrate-covered water body ranged from 16 to 1020 mg/L, and the electrical conductivity varied between 898 and 5594 $\mu\text{s}/\text{cm}$. The floating sphere cover was most effective in inhibiting bottom sediment re-suspension at wind speeds between 3.3 m/s and 7.8 m/s, with suspended sediment concentrations reduced by 12.29–36.98 % and conductivity decreased by 12.51–41.26 %. At wind speeds classified as Class I (≤ 1.5 m/s), the floating sphere cover reduces airborne sand and dust deposition, leading to a significant decrease in the concentration of suspended solids on the water surface. Specifically, the concentration of suspended solids is reduced by 21.95 %, and the conductivity decreases by 16.2 %.

The conductivity and suspended solids concentration data indicate that at wind speeds of Class V (≥ 10.7 m/s), the turbulence in the water becomes severe, and the floating sphere cover is unable to mitigate the disturbance caused by wind and waves on the bottom sediment. However, it effectively prevents sudden increases in surface water salinity caused by sand and dust deposition, reducing suspended solids concentrations by 11.59–15.29 % and conductivity values by 7.75–23.06 %.

3.5.2. Wind speed correlation with suspended solids concentration and conductivity

On the same day, we collected data on bottom sediment resuspension under only one wind speed class to prevent the deposition of suspended particles from affecting the fitting results. Water turbidity and conductivity corresponding to the same wind speed intensity were then averaged and analyzed for correlation, as shown in Fig. 14.

The curve fitting of suspended solids concentration with wind speed showed a positive correlation between both water turbidity and

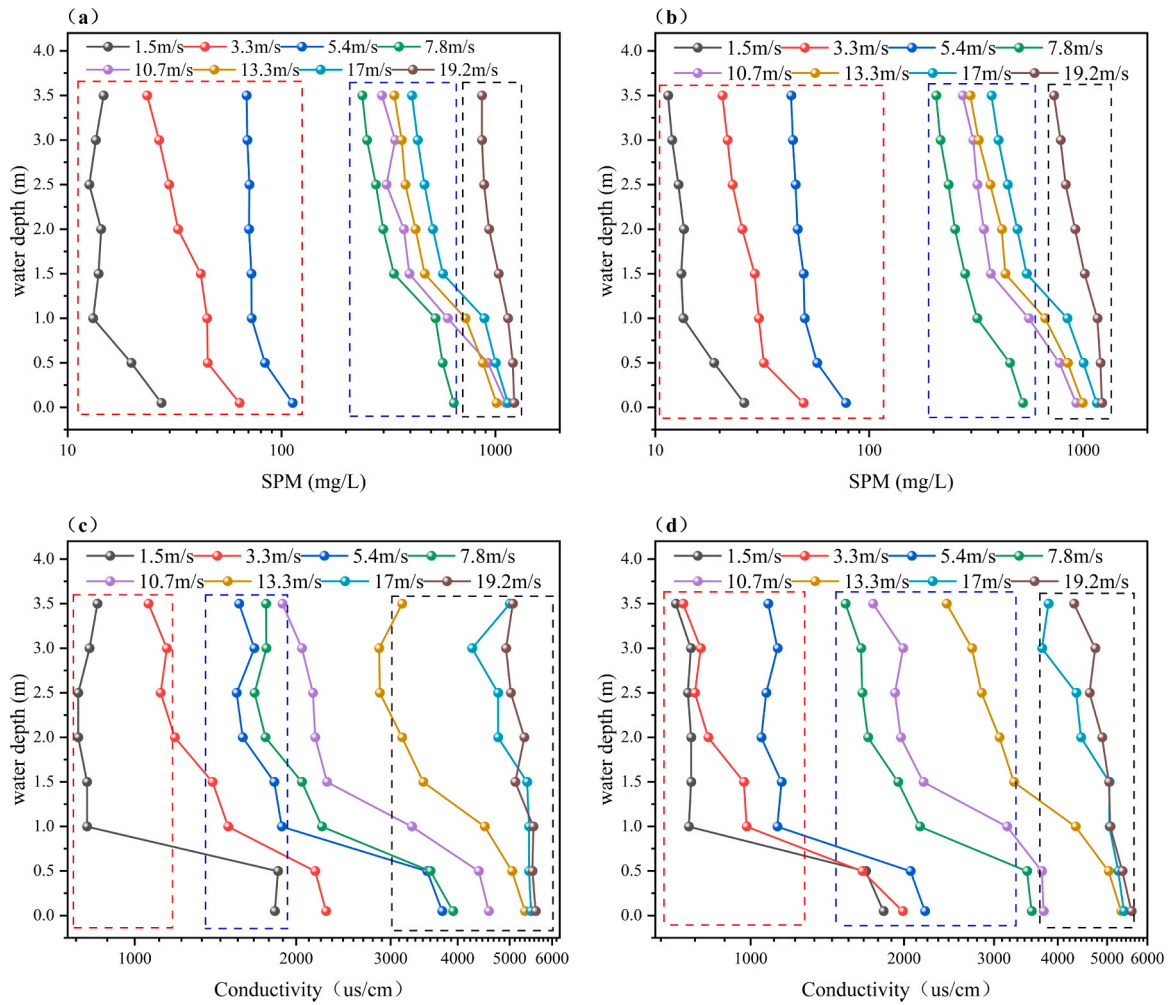


Fig. 12. Vertical distribution of suspended solids concentration and water conductivity at different water depths and wind speeds, where (a) is the concentration of uncovered suspended solids, (b) is the concentration of covered suspended solids, (c) is the conductivity of uncovered water, and (d) is the conductivity of covered water. Water depth is the distance from this layer of water to the bottom sediment.

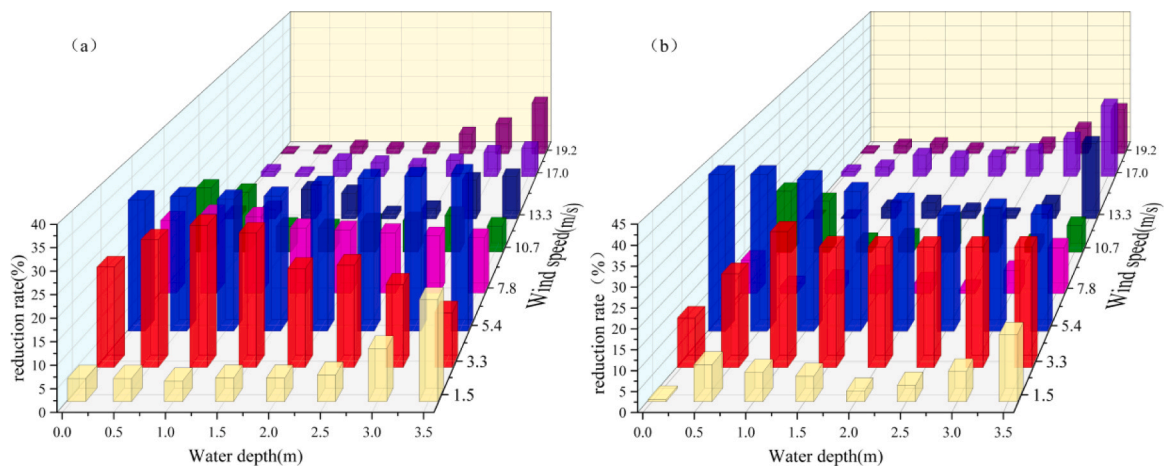


Fig. 13. (a) Reduction rate of suspended solids content in the water body at different depths after floating sphere coverage, (b) Reduction rate of conductivity content in the water body at different depths after floating sphere coverage. Different colored columns represent different wind speed classes and Water depth is the distance to the bottom sediment in the water body at different depths.

conductivity and the wind speed. For the uncovered case, the relationship between suspended solids concentration and wind speed followed an exponential function, with a correlation of $R^2 = 0.901$ (Fig. 14a). In

contrast, when the water surface was covered with floating spheres, the relationship between suspended solids concentration and wind speed was better described by a power function, with a correlation of R^2

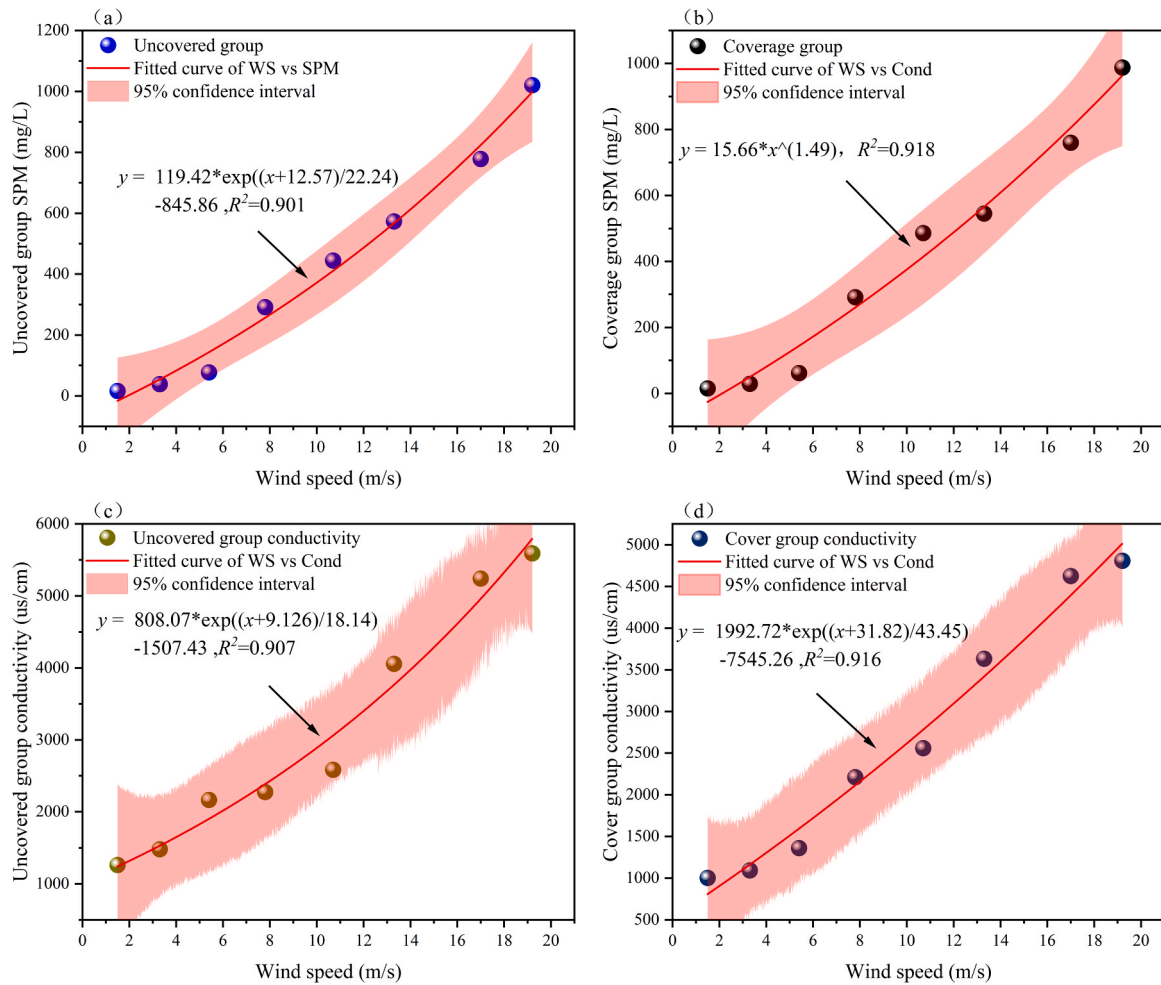


Fig. 14. Correlation between average turbidity of water body and wind speed, in which (a) is correlation between average concentration of suspended solids in uncovered water body and wind speed at different wind speeds; (b) The correlation between the average concentration of suspended solids in water body and wind speed under different wind speeds; (c) The correlation between the average conductivity of uncovered water body and wind speed at different wind speeds; (d) The correlation between the average conductivity of water body and wind speed under different wind speeds. Each data set is the mean of 3 measurements, and the p-value for each sample measurement is ≤ 0.05 .

= 0.918 (Fig. 14b). Additionally, when the water body was disturbed by wind and waves, the conductivity of the water showed an exponential relationship with wind speed, with $R^2 = 0.907$ for the uncovered group

and $R^2 = 0.916$ for the covered group. As shown in Fig. 14 (c) and (d), both the concentration of suspended solids and electrical conductivity are strongly correlated with wind speed. Therefore, wind speed can

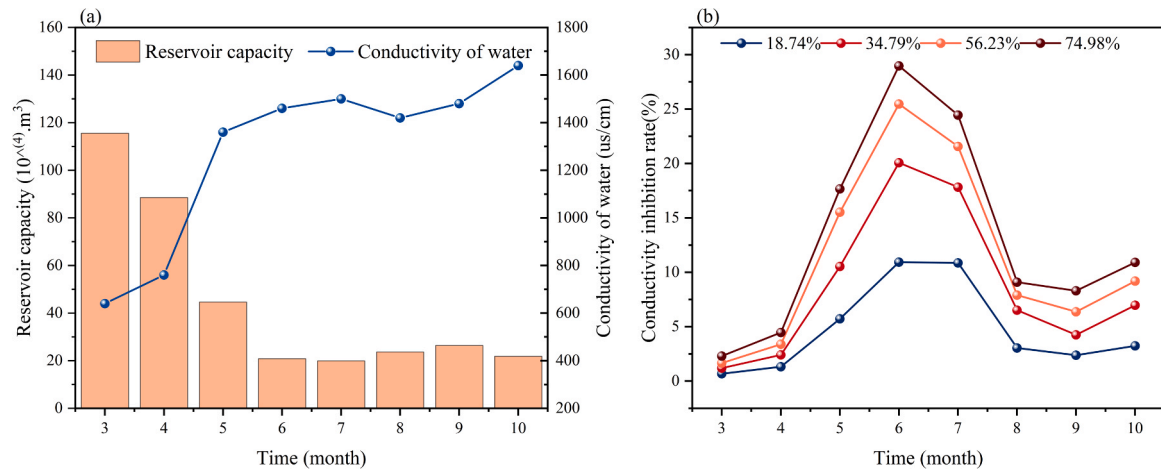


Fig. 15. (a) Reservoir capacity and conductivity under different months, (b) Estimated reduction in conductivity values of the reservoir water body under different floating sphere coverages, with the percentages in the legend representing different floating sphere coverage areas.

serve as an indicator of the conductivity value of the water body when disturbed by wind and waves under specific conditions.

3.6. Estimation of reservoir salt concentration under floating sphere coverage

The conductivity of the reservoir water body was monitored through monthly sampling and analysis, with the results for both the monthly reservoir capacity and water conductivity throughout a complete irrigation cycle shown in Fig. 15(a). Taking into account the corresponding monthly reservoir water level, capacity, and evaporation from the reservoir surface (measured using a $\Phi 20$ evaporation dish), the dilution of the salt concentration in the water body due to different coverage levels of floating spheres was calculated, as shown in Fig. 15(b).

When the water surface was covered with floating spheres (18.74–74.98 %) to inhibit evaporation, the salt concentration in the water body was reduced by an average of 4.77–13.26 % throughout one irrigation cycle. The maximum reduction in salt concentration was 28.97 % ($P < 0.05$), observed when 74.98 % of the water surface was covered, effectively inhibiting evaporation. The accumulation of salt concentration in the reservoir's water body due to evaporation and concentration is a gradual process. Since the lifespan of high-density polyethylene (HDPE) floats can exceed 20 years, using these floats to cover the water surface for extended periods can effectively reduce salt concentrations in the reservoir water and help prevent the salinization of the water body.

4. Discussion

4.1. Release of bottom sediment salts under floating sphere coverage

Monitoring the conductivity of the water body at the early stage of water intake in the evaporator reveals that during this period, the bottom sediment becomes fully saturated, and the exchange of salts between the sediment and the water body plays a significant role in the salinization process. As the salinity gradient between the overlying water and the pore water in the sediment decreases, the rate of salt release from the sediment to the overlying water gradually declines. Consequently, evapotranspiration and concentration become the dominant factors contributing to the increase in salt concentration. Therefore, long-term inhibition of evaporation by covering the water body can effectively mitigate the salinization of the reservoir area.

Additionally, the release of salts from bottom sediments to the overlying water is a long-term, recurring process (Jeppesen et al., 2005). Long-term monitoring data on total phosphorus from 35 lakes, compared to predictions from the Vollenweider equation, suggests that endogenous sources from lake sediments influence the water column's salt levels throughout 10–15 years. (Katsev and Dittrich, 2013) compared modeling and field monitoring results for Lake Sempach, suggesting that approximately 66 % of phosphorus nutrient release from the top 10 cm of sediments can take up to 20 years. The time scale for the impact of bottom sediments on overlying water quality is even longer when the exchange between surface water and groundwater is taken into account. (Lerman and Jones, 1973) modeled transient and steady-state salt diffusion between sediment and lake water in a closed lake, predicting that it would take 6×10^5 years for the salt concentrations in the lake water to stabilize.

(Hurwitz et al., 2000) developed a one-dimensional solute transport model that incorporates convection, diffusion, and sediment compaction. Their model predicted that it would take 2.5×10^3 years for the thickness of the salt diffusion gradient zone to increase from 12 to 23 m. This finding helps explain the 56.95 % contribution to the increase in salt concentration caused by bottom sediments in October, despite the release of salts from the bottom sediment into the overlying water column after just one irrigation cycle in a small-scale evaporator.

When the water surface was covered with 74.98 % floating spheres,

the salt concentration in the water body was reduced by 32.09 % over seven months (March to October). By suppressing evaporation from the water body over an extended period, this approach helps reduce the salinity of downstream irrigation water, thereby safeguarding crop yields. It also contributes to lowering the accumulation of salts in the bottom sediment and mitigating the salinization of the reservoir water.

4.2. Effect of various water quality parameters on salt transport under floating sphere coverage

4.2.1. Effect of water temperature on salt transport under float coverage

The impact of anti-evaporation covers on water temperature depends on factors such as the coverage area, thermal conductivity, water depth, and atmospheric conditions. For shallower water bodies (less than 30 cm), covering them with mulch may lead to increased water temperatures (Shalaby et al., 2024, 2021). In contrast, the higher thermal conductivity of the mulch enables gradual heating of deeper water bodies (Mady et al., 2021). In this experiment, the floating spheres covering the water surface reduced the temperature of the bottom water column, which aligns with the findings of (Aminzadeh et al., 2018), who simulated daily temperature distribution in a 10-meter deep reservoir covered with foam discs using meteorological data. This temperature reduction is attributed to the low thermal conductivity of the cover ($0.13 \text{ W}\cdot\text{m}^{-1}\cdot\text{K}^{-1}$ for HDPE floating spheres) and the considerable water depth. Lower temperatures in the bottom water column can help inhibit the release of salt concentrations from the bottom sediment in the reservoir.

4.2.2. Effect of dissolved oxygen and pH on salt migration in floating sphere covered water

The release of salts from bottom sediments is primarily influenced by dissolved oxygen and pH levels in the water column, which affect the redox reactions at the soil-water interface. In anoxic conditions, the decomposition of organic matter in the bottom sediments enhances denitrification, promoting the release of NH_4^+ . The mineralization of organic nitrogen leads to the production of highly soluble $\text{NH}_4^+\text{-N}$, which increases nutrient salt concentrations in the water column (Bareha et al., 2018; Qin et al., 2004). When dissolved oxygen levels in the water column are high, Fe^{2+} and Al^{3+} undergo oxidation reactions to form iron and aluminum oxides (Nguyen, 1999; Qin et al., 2004), converting amorphous iron oxides into crystalline iron and aluminum oxides. In such conditions, phosphorus in the water column is less likely to be released again, as it reacts with crystalline iron oxides, aluminum oxides, or calcium carbonate through precipitation, or binds with more resistant organic matter like humic acid (Rydin, 2000; Saavedra and Delgado, 2005; Peng et al., 2007).

When the water pH is neutral, it creates a favorable environment for nitrogen-consuming microorganisms, weakens the redox reactions of metal ions, and inhibits the release of nutrient salts from the substrate (Kraal et al., 2009). In contrast, in acidic or alkaline environments, stronger redox reactions occur at the soil-water interface, such as the conversion of ammonium (NH_4^+) into ammonia gas (NH_3) and the formation of hydroxide ions (OH^-) (Zhang et al., 2014). Phosphate ions in these conditions will react with metal ions to form insoluble precipitates, such as tricalcium phosphate ($\text{Ca}_3(\text{PO}_4)_2$) and aluminum phosphate (AlPO_4) (Kraal et al., 2009). This increases the concentration gradient of nitrogen and phosphorus nutrients at the soil-water interface, promoting the release of these nutrients from the subsoil sediments.

Due to the gaps between the floating spheres, the water surface covered with floating spheres did not experience a significant decrease in dissolved oxygen levels in the water column, unlike the effect observed with shade nets (Maestre-Valero et al., 2011). For the evaporator covered with 74.98 % floating spheres, the lowest dissolved oxygen concentration of 6.58 mg/L occurred in July, which remains above the survival threshold for aquatic plants and animals, ensuring no harm

to them (Duc et al., 2016). Compared to uncovered evaporators, the decrease in dissolved oxygen at maximum water surface coverage was minimal, which may have contributed to a slight increase in salt release from the bottom sediment. The primary factor influencing changes in water pH was the concentration of carbon dioxide in the water column, which rose during the summer months when algae photosynthesis was active, leading to the consumption of carbon dioxide. As the coverage of floating spheres on the water surface increases, the photosynthesis of aquatic plants is reduced while respiration is enhanced. This leads to a rise in carbon dioxide concentration in the water, causing a decrease in pH. In this experiment, the pH of the water body in the covered groups tended to be closer to neutral, which helps to slow down the release of salts from the bottom sediment.

4.3. Inhibition of re-suspension of bottom sediment by floating sphere coverage

The effectiveness of floating sphere coverage in inhibiting the re-suspension of bottom sediment depends on the critical wind speed required for sediment re-suspension. Studies by (Qin et al., 2004) have shown that in wide, shallow water bodies like plain reservoirs in arid regions, suspended sediment concentration increases significantly during Class IV winds (5.5–7.9 m/s). This suggests that such wind speeds are sufficient to reach the critical threshold for sediment re-suspension in the water body. In this test, the 400 m² area covered by floating spheres effectively inhibited bottom sediment re-suspension within the wind speed range of 3.3 m/s to 7.8 m/s. However, when the wind speed reached or exceeded 10.7 m/s, the bottom sediment surpassed the critical wind speed for re-suspension, and the floating spheres ability to inhibit sediment disturbance was significantly reduced. (Zhou et al., 2018) observed similar trends in Lake Taihu, where the concentration of suspended matter in the bottom water layer, under strong wind and wave disturbance, was 3–5 times higher than that in the upper water layer. According to the vertical distribution of water conductivity, when the wind speed exceeds class V, the conductivity of the uncovered surface water increases significantly. However, in the covered water body with floating spheres, the surface water conductivity remained lower than that of the deeper water layers. This is because the floating sphere cover prevents sand and dust from directly entering the water, thus mitigating sudden increases in surface water salinity. Additionally, the duration and direction of the wind, along with the surrounding geography of the water body, can influence the extent to which the wind affects the resuspension of bottom sediment.

Similar to the findings of Cózar et al. (2005) and (You et al., 2007) regarding the correlation between wind speed and suspended sediments, both wind speed and water turbidity in our study showed an exponential relationship. This suggests that the re-suspension of bottom sediments induced by wind speed is non-linear, potentially linked to the wave strength or critical wind speed needed for the secondary suspension of bottom sediment. In our monitoring, wind speed was positively correlated with water turbidity, which differs from the inverse relationship observed by Cózar et al. (2005). They proposed that this paradox might arise from particles aggregating around sensors, which are then displaced as wind speed increases. However, sediment re-suspension does not occur until significant wave development takes place.

4.4. Evaporation suppression and cost-benefit analysis

Regarding evaporation inhibition efficiency, existing studies show that chemical film coverage ranges from 7 % to 40 %, while shade nets and polyethylene foam disks achieve approximately 80 % coverage when the water surface is fully covered (Lehmann et al., 2019). Due to the excellent mechanical properties of floating spheres, which prevent stacking and loss of coverage area, they offer a significantly higher anti-evaporation inhibition rate (approximately 70 % when the water surface is covered by 74.98 %) (Aminzadeh et al., 2018; Han et al.,

2020). Additionally, the floating spheres have a service life of up to 20 years, making them more effective in reducing evaporation and preventing salt concentration in the water body. In terms of cost-effectiveness, the payback period can be reduced to less than two years when the indirect benefits from water-saving irrigation for crops (locally grown grapes) are considered (Hao et al., 2023). Additionally, the floating sphere cover has low maintenance costs; if a floating sphere breaks, it only requires the addition of a new sphere to the water surface.

4.5. Effects of groundwater erosion and substrate disturbance on reservoir salt concentrations

According to the Annual Report on Shallow Groundwater Dynamics in Turpan, the groundwater depth in the test area exceeds 14 m (Chen et al., 2014), meaning groundwater does not directly recharge the reservoir water. Therefore, the effect of groundwater-induced salt erosion was not considered in this study. The floating spheres covering 400 m² of the water surface effectively inhibited sediment re-suspension at wind speeds of up to 7.8 m/s. However, due to varying water depths and meteorological factors such as wind speed, direction, and temperature, the impact of a larger floating sphere coverage or full coverage on salt release through sediment re-suspension remains unclear. Consequently, Section 3.6 focuses only on estimating the effect of evaporation inhibition on reducing salt concentration in the entire reservoir area.

4.6. Study limitations

We conducted the study for only one irrigation cycle, which is a relatively short period, so long-term observation at the reservoir scale is necessary. Additionally, the wind displacement of the floating sphere cover group should be considered in the reservoir's field environment, and the cover needs to be secured in alignment with the site's topography. There is also a lack of research on the potential ecological impacts of prolonged floating sphere coverage on aquatic organisms, and further investigation is needed.

5. Conclusion

Monitoring of salt concentrations in the five evaporators indicates that, for reservoirs that have been in operation for extended periods, evaporative concentration significantly contributes to salt accumulation. The floating spheres covering the water surface help reduce water temperatures and maintain near-neutral pH levels, which aids in inhibiting the release of salts from the bottom sediments. While the reduction in dissolved oxygen in the water column may promote the release of salts, the gaps between the floating spheres allow for the replenishment of dissolved oxygen, preventing hypoxia in the water. When the wind speed ranges from 3.3 m/s to 7.8 m/s, floating spheres covering the water surface effectively suppress sediment resuspension. Additionally, during windy conditions, the floating spheres prevent an increase in surface water salinity caused by dust deposition into the water body. Focusing solely on the evapotranspiration concentration effect, covering the water surface with 74.98 % floating spheres to inhibit evaporation results in a 28.97 % reduction in salt concentration within one full irrigation cycle (March to October). Regarding the coverage of the water surface with floating spheres, it should be tailored to the specific conditions at the reservoir site. In field applications, a floating box fence is used to gather the floating spheres together. This study demonstrates that floating HDPE spheres effectively reduce evaporation and mitigate salinity, with a 28.97 % reduction over one irrigation cycle ($p < 0.05$). However, challenges such as wind displacement, long-term durability, and economic feasibility must be addressed before large-scale implementation. Future research should focus on multi-year assessments, cost-benefit analyses, and environmental sustainability considerations. This approach of using floating spheres to inhibit evaporation offers a simple, convenient, and effective

solution for mitigating the salinization of reservoirs.

CRedit authorship contribution statement

Han Ke-wu: Software, Resources. **Shi Ke Bin:** Methodology, Funding acquisition. **Hao Guo-chen:** Writing – review & editing, Writing – original draft, Visualization, Validation, Supervision, Software, Resources, Project administration, Methodology, Investigation, Funding acquisition, Formal analysis, Data curation, Conceptualization.

Declaration of Competing Interest

The authors declare that they have no known competing financial interests or personal relationships that could have appeared to influence the work reported in this paper.

Acknowledgements

Acknowledgments: We extend our appreciation to the Researchers Supporting Project at Xinjiang Key Laboratory Research Project on Hydraulic Engineering Safety and Water Control Prevention (Project No. ZDSYS-YIS-2021-01), and the Xinjiang Agricultural University Graduate School-level Research and Innovation Program (Project No. XJAUGR2023001).

Appendix A. Supporting information

Supplementary data associated with this article can be found in the online version at doi: [10.1016/j.agwat.2025.109440](https://doi.org/10.1016/j.agwat.2025.109440)

Data availability

Data will be made available on request.

References

- Abdallah, A.M., Parihar, C.M., Patra, S., Nayak, H.S., Saharawat, Y.S., Singh, U., Parihar, M.D., Kakraliya, S.K., Nassar, I.N., Ugolini, F., 2021. Critical evaluation of functional aspects of evaporation barriers through environmental and economics lens for evaporation suppression—a review on milestones from improved technologies. *Sci. Total Environ.* 788, 147800. <https://doi.org/10.1016/j.scitotenv.2021.147800>.
- Althoff, D., Filgueiras, R., Rodrigues, L.N., 2020a. Estimating small reservoir evaporation using machine learning models for the Brazilian Savannah. *J. Hydrol. Eng.* 25, 05020019. [https://doi.org/10.1061/\(ASCE\)HE.1943-5584.0001976](https://doi.org/10.1061/(ASCE)HE.1943-5584.0001976).
- Althoff, D., Rodrigues, L.N., Da Silva, D.D., 2020b. Impacts of climate change on the evaporation and availability of water in small reservoirs in the Brazilian savannah. *Clim. Change* 159, 215–232. <https://doi.org/10.1007/s10584-020-02656-y>.
- Aminzadeh, M., Lehmann, P., Or, D., 2018. Evaporation suppression and energy balance of water reservoirs covered with self-assembling floating elements. *Hydrol. Earth Syst. Sci.* 22, 4015–4032. <https://doi.org/10.5194/hess-22-4015-2018>.
- Bareha, Y., Girault, R., Jimenez, J., Tremier, A., 2018. Characterization and prediction of organic nitrogen biodegradability during anaerobic digestion: a bioaccessibility approach. *Bioresour. Technol.* 263, 425–436. <https://doi.org/10.1016/j.biortech.2018.04.085>.
- Cary, L., Petelet-Giraud, E., Bertrand, G., Kloppmann, W., Aquilina, L., Martins, V., Hirata, R., Montenegro, S., Pauwels, H., Chatton, E., 2015. Origins and processes of groundwater salinization in the urban coastal aquifers of Recife (Pernambuco, Brazil): a multi-isotope approach. *Sci. Total Environ.* 530, 411–429. <https://doi.org/10.1016/j.scitotenv.2015.05.015>.
- Chen, L., Wang, G., Hu, F., Wang, Y., Liu, L., 2014. Groundwater hydrochemistry and isotope geochemistry in the Turpan Basin, northwestern China. *J. Arid Land* 6, 378–388. <https://doi.org/10.1007/s40333-013-0249-9>.
- Cózar, A., Gálvez, J.A., Hull, V., García, C.M., Loiselle, S.A., 2005. Sediment resuspension by wind in a shallow lake of Esteros del Ibera (Argentina): a model based on turbidity. *Ecol. Model.* 186, 63–76. <https://doi.org/10.1016/j.ecolmodel.2005.01.020>.
- Craig, I., Green, A., Scobie, M., Schmidt, E., 2005. Controlling Evaporation Loss from Water Storages. University of Southern Queensland. <https://research.usq.edu.au/item/9y3q1/controlling-evaporation-loss-from-water-storages>.
- Cui, Y., Shao, J., 2005. The role of ground water in arid/semiarid ecosystems, Northwest China. *Groundwater* 43, 471–477. <https://doi.org/10.1111/j.1745-6584.2005.0063.x>.
- Duc, V.N., Bac, N.A., Hoang, T.H.T., 2016. Dissolved oxygen as an indicator for eutrophication in freshwater lakes. In: Proceedings of the International Conference on Environmental Engineering and Management for Sustainable Development. https://www.researchgate.net/publication/308991144_Dissolved_Oxygen_as_an_Indicator_for_Eutrophication_in_Freshwater_Lakes.
- El-Ghannam, M.K., Aiad, M.A., Abdallah, A.M., 2021. Irrigation efficiency, drain outflow and yield responses to drain depth in the Nile delta clay soil, Egypt. *Agric. Water Manag.* 246, 106674. <https://doi.org/10.1016/j.agwat.2020.106674>.
- El-Shirbeny, M.A., Abutaleb, K.A., 2018. Monitoring of water-level fluctuation of Lake Nasser using altimetry satellite data. *Earth Syst. Environ.* 2, 367–375. <https://doi.org/10.1007/s41748-018-0053-y>.
- Fan, G., Bao, S., Guo, Y., Xia, M., Lin, M., Cai, S., Ruan, W., Liao, T., Yan, Z., 2022. Spatio-temporal variations of salinity and analysis of desalination factors in a Chinese coastal storage reservoir. *Process Saf. Environ. Prot.* 159, 26–35. <https://doi.org/10.1016/j.psep.2021.12.052>.
- Friedrich, K., Grossman, R.L., Huntington, J., Blanken, P.D., Lenters, J., Holman, K.D., Gochis, D., Livneh, B., Prairie, J., Skeie, E., 2018. Reservoir evaporation in the Western United States: current science, challenges, and future needs. *Bull. Am. Meteorol. Soc.* 99, 167–187. <https://doi.org/10.1175/BAMS-D-15-00224.1>.
- Gassama, N., Dia, A., Violette, S., 2012. Origin of salinity in a multilayered aquifer with high salinization vulnerability. *Hydrol. Process* 26, 168–188. <https://doi.org/10.1002/hyp.8125>.
- Gebrehiwet, M., Tafesse, N.T., Habtu, S., Alemaw, B.F., Laletsang, K., Lasarwe, R., 2021. The contribution of groundwater to the salinization of reservoir-based irrigation systems. *Agronomy* 11, 512. <https://doi.org/10.3390/agronomy11030512>.
- Grünberger, O., Macaigne, P., Michelot, J.-L., Hartmann, C., Sukchan, S., 2008. Salt crust development in paddy fields owing to soil evaporation and drainage: contribution of chloride and deuterium profile analysis. *J. Hydrol.* 348, 110–123. <https://doi.org/10.1016/j.jhydrol.2007.09.039>.
- Hammecker, C., Maecht, J.-L., Grünberger, O., Siltacho, S., Srisruk, K., Noble, A., 2012. Quantification and modelling of water flow in rain-fed paddy fields in NE Thailand: evidence of soil salinization under submerged conditions by artesian groundwater. *J. Hydrol.* 456, 68–78. <https://doi.org/10.1016/j.jhydrol.2012.06.005>.
- Han, K.-W., Shi, K.-B., Yan, X.-J., 2020. Evaporation loss and energy balance of agricultural reservoirs covered with counterweighted spheres in arid region. *Agric. Water Manag.* 238, 106227. <https://doi.org/10.1016/j.agwat.2020.106227>.
- Hao, G., Han, K., Shi, K., 2023. Effect of floating spheres on evaporation inhibition, surface energy balance and biological water quality parameters at different coverage fractions. *Agric. Water Manag.* 287, 108460. <https://doi.org/10.1016/j.agwat.2023.108460>.
- Hayashi, M., 2004. Temperature-electrical conductivity relation of water for environmental monitoring and geophysical data inversion. *Environ. Monit. Assess.* 96, 119–128. <https://doi.org/10.1023/B:EMAS.0000031719.83065.68>.
- Hurwitz, S., Lyakhovskiy, V., Gvirtzman, H., 2000. Transient salt transport modeling of shallow brine beneath a freshwater lake, the Sea of Galilee, Israel. *Water Resour. Res.* 36, 101–107. <https://doi.org/10.1029/1999WR900292>.
- Jeppesen, E., Søndergaard, M., Jensen, J.P., Havens, K.E., Anneville, O., Carvalho, L., Coveney, M.F., Deneke, R., Dokulil, M.T., Foy, B., Gerdeaux, D., Hampton, S.E., Hilt, S., Kangur, K., Köhler, J., Lammens, E.H.H.R., Lauridsen, T.L., Manca, M., Miracle, M.R., Moss, B., Nøges, P., Persson, G., Phillips, G., Portielje, R., Romo, S., Schelske, C.L., Straile, D., Tatrai, I., Willén, E., Winder, M., 2005. Lake responses to reduced nutrient loading – an analysis of contemporary long-term data from 35 case studies. *Freshw. Biol.* 50, 1747–1771. <https://doi.org/10.1111/j.1365-2427.2005.01415.x>.
- Katsev, S., Ditttrich, M., 2013. Modeling of decadal scale phosphorus retention in lake sediment under varying redox conditions. *Ecol. Model.* 251, 246–259. <https://doi.org/10.1016/j.ecolmodel.2012.12.008>.
- Kraal, P., Slomp, C.P., Forster, A., Kuypers, M.M., Sluijs, A., 2009. Pyrite oxidation during sample storage determines phosphorus fractionation in carbonate-poor anoxic sediments. *Geochim. Cosmochim. Acta* 73, 3277–3290. <https://doi.org/10.1016/j.gca.2009.02.026>.
- Lehmann, P., Aminzadeh, M., Or, D., 2019. Evaporation suppression from water bodies using floating covers: laboratory studies of cover type, wind, and radiation effects. *Water Resour. Res.* 55, 4839–4853. <https://doi.org/10.1029/2018WR024489>.
- Lerman, A., Jones, B.F., 1973. Transient and steady-state salt transport between sediments and brine in closed Lakes 1. *Limnol. Oceanogr.* 18, 72–85. <https://doi.org/10.4319/lo.1973.18.1.0072>.
- Li, C.-L., Shi, K.-B., Yan, X.-J., Jiang, C.-L., 2021. Experimental analysis of water evaporation inhibition of plain reservoirs in inland arid area with light floating spheres and floating plates in Xinjiang, China. *J. Hydrol. Eng.* 26, 04020060. [https://doi.org/10.1061/\(ASCE\)HE.1943-5584.0002032](https://doi.org/10.1061/(ASCE)HE.1943-5584.0002032).
- Mady, B., Lehmann, P., Or, D., 2021. Evaporation suppression from small reservoirs using floating covers—field study and modeling. *Water Resour. Res.* 57, e2020WR028753. <https://doi.org/10.1029/2020WR028753>.
- Maestre-Valero, J.F., Martínez-Alvarez, V., Gallego-Elvira, B., Pittaway, P., 2011. Effects of a suspended shade cloth cover on water quality of an agricultural reservoir for irrigation. *Agric. Water Manag.* 100, 70–75. <https://doi.org/10.1016/j.agwat.2011.08.020>.
- Merchán, D., Auké, L.F., Acero, P., Gimeno, M.J., Causapé, J., 2015. Geochemical processes controlling water salinization in an irrigated basin in Spain: identification of natural and anthropogenic influence. *Sci. Total Environ.* 502, 330–343. <https://doi.org/10.1016/j.scitotenv.2014.09.041>.
- Mongelli, G., Monni, S., Oggiano, G., Paternoster, M., Sinisi, R., 2013. Tracing groundwater salinization processes in coastal aquifers: a hydrogeochemical and isotopic approach in the Na-Cl brackish waters of northwestern Sardinia, Italy. *Hydrol. Earth Syst. Sci.* 17, 2917–2928. <https://doi.org/10.5194/hess-17-2917-2013>, 2013.

- Nguyen, L.M., 1999. Phosphate incorporation and transformation in surface sediments of a sewage-impacted wetland as influenced by sediment sites, sediment pH and added phosphate concentration. *Ecol. Eng.* 14, 139–155. [https://doi.org/10.1016/S0925-8574\(99\)00025-7](https://doi.org/10.1016/S0925-8574(99)00025-7).
- Peng, J., Wang, B., Song, Y., Yuan, P., Liu, Z., 2007. Adsorption and release of phosphorus in the surface sediment of a wastewater stabilization pond. *Ecol. Eng.* 31, 92–97. <https://doi.org/10.1016/j.ecoleng.2007.06.005>.
- Qin, B., Hu, W., Gao, G., Luo, L., Zhang, J., 2004. Dynamics of sediment resuspension and the conceptual schema of nutrient release in the large shallow Lake Taihu, China. *Chin. Sci. Bull.* 49, 54–64. <https://doi.org/10.1007/BF02901743>.
- Rocha, J., Carvalho-Santos, Cláudia, Diogo, P., Bea, P., Nunes, J.P., 2020. Impacts of climate change on reservoir water availability, quality and irrigation needs in a water scarce Mediterranean region (southern Portugal). *Sci. Total Environ.* 736, 139477. <https://doi.org/10.1016/j.scitotenv.2020.139477>.
- Rydin, E., 2000. Potentially mobile phosphorus in Lake Erken sediment. *Water Res.* 34, 2037–2042. [https://doi.org/10.1016/S0043-1354\(99\)00375-9](https://doi.org/10.1016/S0043-1354(99)00375-9).
- Saavedra, C., Delgado, A., 2005. Iron-related phosphorus in eroded sediments from agricultural soils of Mediterranean areas. *Geoderma* 125, 1–9. <https://doi.org/10.1016/j.geoderma.2004.06.001>.
- Shalaby, M.M., Nassar, I.N., Abdallah, A.M., 2021. Evaporation suppression from open water surface using various floating covers with consideration of water ecology. *J. Hydrol.* 598, 126482. <https://doi.org/10.1016/j.jhydrol.2021.126482>.
- Shalaby, M.M., Nassar, I.N., Abdallah, A.M., 2024. Effect of continuous and modular floating covers on evaporation losses and microalgal growth. *J. King Saud. Univ. Eng. Sci.* 36, 23–31. <https://doi.org/10.1016/j.jksues.2021.08.007>.
- Shrivastava, P., Kumar, R., 2015. Soil salinity: A serious environmental issue and plant growth promoting bacteria as one of the tools for its alleviation. *Saudi J. Biol. Sci.* 22, 123–131. <https://doi.org/10.1016/j.sjbs.2014.12.001>.
- Spinoni, J., Micale, F., Carrao, H., Naumann, G., Barbosa, P., Vogt, J., 2013. Global and continental changes of arid areas using the FAO Aridity Index over the periods 1951–1980 and 1981–2010. in: EGU General Assembly Conference Abstracts, EGU2013-9262. [https://doi.org/10.1016/S0165-0114\(95\)00340-1](https://doi.org/10.1016/S0165-0114(95)00340-1).
- You, B., Zhong, J., Fan, C., Wang, T., Zhang, L., Ding, S., 2007. Effects of hydrodynamics processes on phosphorus fluxes from sediment in large, shallow Taihu Lake. *J. Environ. Sci.* 19, 1055–1060. [https://doi.org/10.1016/S1001-0742\(07\)60172-7](https://doi.org/10.1016/S1001-0742(07)60172-7).
- Yuan, R., Wang, S., Yang, L., Liu, J., Wang, P., Song, X., 2018. Hydrologic processes of groundwater in a small monsoon-influenced mountainous watershed. *Hydrol. Res.* 49, 2016–2029. <https://doi.org/10.2166/nh.2018.030>.
- Zaman, M., Shahid, S.A., Heng, L., 2018. Guideline for Salinity Assessment, Mitigation and Adaptation Using Nuclear and Related Techniques. Springer Nature. <https://doi.org/10.1007/978-3-319-96190-3>.
- Zhang, L., Wang, S., Wu, Z., 2014. Coupling effect of pH and dissolved oxygen in water column on nitrogen release at water–sediment interface of Erhai Lake, China. *Estuar. Coast. Shelf Sci.* 149, 178–186. <https://doi.org/10.1016/j.ecss.2014.08.009>.
- Zhou, Y., Liu, J., Xu, X., Qi, C., Wu, X., Liu, H., Shi, K., 2018. Response of suspended solids and dissolved nutrients in littoral zone of Lake Taihu under wind-wave disturbances. *J. Lake Sci.* 30, 948–956. <https://doi.org/10.18307/2018.0408>.
- Zhu, L., Jiang, C., Zhang, P., Li, D., Zhu, X., 2015. Eutrophication in the newly built Laohutan Reservoir during the initial impoundment period: the role of nutrient loading. *Environ. Earth Sci.* 74, 4803–4812. <https://doi.org/10.1007/s12665-015-4469-5>.